Phosphate removal from aqueous solution by Fe-La binary (hydr)oxides: A study of batch experiments and mechanisms

Haijing Duan
Henan University
Lin Zhang
Henan University
Yu-long Wang (365457715@qq.com)
Henan University
Yanhong Liu
Henan University
Yangyang Wang
Henan University

Research Article

Keywords: Fe-La binary (hydr)oxides, Phosphate, Rhabdophane, Removal, Adsorption

Posted Date: April 20th, 2021

DOI: https://doi.org/10.21203/rs.3.rs-396802/v1

Abstract

In this study, Fe-La binary (hydr)oxides were prepared by a co-precipitation method for phosphate removal. Various techniques, including secondary electron microscopy with energy dispersive X-ray spectroscopy (SEM-EDX), powder X-ray diffraction (p-XRD) and Brunauer-Emmett-Teller (BET) surface area analysis, were employed to characterize the synthesized Fe-La binary (hydr)oxides. Batch experiments indicated that the performance of phosphate removal by Fe-La binary (hydr)oxides was excellent and increased with increasing La contents. The kinetics study showed that the adsorption was rapid and described better by the pseudo-second-order equation. The maximum adsorption capacities of Fe/La 3:1, Fe/La 1:1 and Fe/La 1:3 binary (hydr)oxides at pH 4.0 calculated by Langmuir model were 49.02, 69.44 and 136.99 mg/g, respectively. The uptake of phosphate was highly affected by solution pH and significantly reduced with the increase of pH value. The analyses of p-XRD, Fourier transform infrared spectroscopy (FTIR) and X-ray photoelectron spectroscopy (XPS) suggested that the predominant mechanisms of phosphate removal involved surface hydroxyl exchange reactions and co-precipitation of released La^{3+} and phosphate ions, which resulted into the formation of amorphous phase of rhabdophane ($LaPO_4 \bullet 0.5H_2O$). The results show great potential for the application on the treatment of phosphate decontamination for their high efficiency of phosphate removal.

Highlights

- Fe–La binary (hydr)oxides were prepared by a co-precipitation method.
- The adsorbents showed the excellent performance of phosphate removal.
- The uptake of phosphate was remarkably dependent on solution pH.
- Surface hydroxyl exchange reactions were the major adsorption mechanisms.
- Co-precipitation of rhabdophane was formed.

Introduction

Phosphorus (P) is an essential nutritional element for the growth and development of algae and other living organisms, while excessive amounts of phosphate due to the inputs from urban and agricultural land runoff have a risk of causing eutrophication, harmful algal blooms and subsequent deterioration of aquatic environments and ecosystems (Conley et al. 2009). Consequently, it is indispensable to remove the excessive phosphate from water bodies. Various treatment technologies for phosphate removal including membrane filtration, adsorption, chemical precipitation, ion-exchange, and biological processes, have been developed over the past decades (Pan et al. 2020, Zhang et al. 2021). Compared with other removal processes, adsorption is attractive due to its high efficiency, cost-effectiveness and sample operation (Qu et al. 2020, Vu &Wu 2020). To date, various kinds of functionalized metal (hydr)oxide-based adsorbents, such as biochar-loaded Ce^{3+}-enriched ultra-fine ceria nanoparticles, $NaLa(CO_3)_2$ decorated magnetic biochar, Fe-Al-Mn trimetal oxide adsorbent, graphene-lanthanum composite, magnetic porous biochar supported $La(OH)_3$ and lanthanum hydroxide nanorods, have been explored

and exhibited enhanced phosphate removal (Chen et al. 2015, Fang et al. 2017, Lu et al. 2013, Qu et al. 2020, Yu et al. 2017, Zhang et al. 2021).

In particular, different bimetallic hydroxide adsorbents have been employed due to their high efficiency for phosphate removal, separation convenience and highly efficient reusability. For example, magnetic $La(OH)_3/Fe_3O_4$ nanocomposites have exhibited a high sorption capacity of 83.5 mg P/g, and strong selectivity for phosphate removal (Wu et al. 2017). Vn et al. synthesized magnetic porous NiLa-layered double oxides with improved phosphate adsorption characteristics and antibacterial activities (Vu &Wu 2020). Zhang et al. reported an Fe-Mn binary oxide adsorbent with an Fe/Mn molar ratio of 6:1 prepared by a simultaneous oxidation and co-precipitation process (Zhang et al. 2009).

Recently, lanthanum (La), a rare earth element, has received enormous attention for its environmental friendliness, low cost and excellent phosphate removal performance. A number of La-based adsorbents have been prepared, including La-doped silica spheres, La(III)-bentonite/chitosan composites, lanthanum modified bentonite clay, a nanoporous material referred to as La_{100}SBA-15 and $La(OH)_3$ loaded magnetic mesoporous nanospheres (Chen et al. 2019, Dithmer et al. 2015, Huang et al. 2014, Xu et al. 2020, Yang et al. 2011). La-based bimetallic hydroxide adsorbents have also been designed and developed (Qu et al. 2020, Vu &Wu 2020, Wu et al. 2017). Xu et al. obtained lanthanum/aluminum-hydroxide composites via co-precipitation and its mechanisms of phosphate removal were investigated by X-ray absorption fine structure (XAFS) spectroscopy (Xu et al. 2017). The results indicated that phosphate preferentially bonded with Al under weakly acidic conditions while tended to associate with La under alkaline conditions, leading to the formation of the inner sphere bidentate-binuclear complexes between La(III) and phosphate. However, less attention has been paid to the phosphate removal by La-Fe bimetallic hydroxide adsorbents. In one study, the activation of lattice oxygen in LaFe (oxy)hydroxides for phosphorus removal and their underlying removal mechanisms were determined by X-ray absorption near edge structure (XANES) and X-ray photoelectron spectroscopy (XPS) (Yu et al. 2019). In that study, La-incorporated La-Fe bimetallic hydroxides were employed. However, the Fe-incorporated La-Fe bimetallic hydroxides were ignored. Therefore, there are still some practical limitations that need to be further researched.

In this paper, a series of Fe-La binary (hydr)oxides with different Fe/La molar ratios were prepared by a facile co-precipitation method and characterized by scanning electron microscope with energy-dispersive X-ray spectrometer (SEM-EDX), Brunauer–Emmett–Teller (BET) surface area analysis, powder X-ray diffraction (p-XRD) and the pH of the point of zero charge (pH_{pzc}). Their performance of phosphate removal was studied by adsorption kinetics, adsorption isotherms, the effect of pH, interactive effects with co-existing ions and reusability, and the removal mechanisms were investigated by p-XRD, Fourier transform infrared spectroscopy (FTIR) and XPS analyses.

Materials And Methods

Materials

All analytic grade reagents and chemicals including $La(NO_3)_3 \cdot 6H_2O$, $Fe(NO_3)_3 \cdot 9H_2O$, NaOH, KH_2PO_4, ascorbic acid and molybdenum acid ammonium were purchased from Sinopharm Chemical Reagent Co. (Shanghai, China) and used without further purification. All reaction glass volumetric flasks and vessels used in the experiments were first cleaned by soaking in a 5% HNO_3 solution for least 24 h and then rinsed several times with deionized (DI) water prior to testing. All working solutions were prepared using DI water. A phosphate stock solution with a concentration of 2.0 g/L was obtained by dissolving KH_2PO_4 in DI water. Separate phosphate working solutions with various initial phosphate concentrations were freshly prepared by diluting the phosphate stock solution using DI water.

Preparation of adsorbents

Fe-La binary (hydr)oxides with various Fe/La molar ratios were synthesized via a facile co-precipitation method. In a typical synthesis, predetermined amounts of $Fe(NO_3)_3 \cdot 9H_2O$ and $La(NO_3)_3 \cdot 6H_2O$ were dissolved in 50 mL DI water under magnetic stirring to obtain a series of Fe-La nitrate solutions with different Fe/La molar ratios. Then, the pH of the solution was raised to ~ 10 within approximately 10 min and kept constant by the dropwise addition of a 1 mol/L NaOH solution. After adjusting the pH, the resulting suspensions were continuously stirred for 2 h. After that, the obtained precipitates were washed several times with DI water and freeze-dried for 24 h. The dried products were ground into a fine powder and stored in a desiccator for further use. Samples were labeled according to their initial Fe/La molar ratios, **Fe/La 3:1**, **Fe/La 1:1** and **Fe/La 1:3**. Pure lanthanum hydroxide was also prepared, and details are provided in the Supplementary Material.

Characterization of adsorbents

The morphologies and surface element distributions of the samples were characterized by a field emission scanning electron microscope with energy-dispersive X-ray spectrometer (SEM-EDX) (Phenom LE, Netherlands). The specific surface areas and pore structures of the materials were measured by N_2 adsorption/desorption using a Micromeritics ASAP 2020 surface area analyzer (Micromeritics ASAP 2020, USA) at 77 K and were calculated by the Brunauer–Emmett–Teller (BET) method with the adsorption branches of the isotherms and Barrett–Joyner–Halenda (BJH) model with the desorption curves, respectively. FTIR spectra were recorded on a Nicolet Nexus 870 FT-IR spectrometer using a transmission model (Nicolet, USA) with the KBr pellet technique. In order to investigate the surface chemistry compositions of the materials before and after phosphate adsorption, X-ray photoelectron spectra (XPS) were collected on an X-ray photoelectron spectra spectrometer (ESCALAB 250Xi, Thermo Fisher, America) equipped with a monochromatized Al Kα X-ray source ($h\nu$ = 1486.6 eV) and a hemispherical electron analyzer. The C 1s photoelectron peak (284.6 eV) was used for calibrating the binding energy. A nonlinear least-squares curve fitting program was employed in the data analysis using XPSPEAK41 Software. The spectral bands were deconvoluted with the subtraction of a nonlinear Shirley-type background and a Gaussian (20%)-Lorentzian (80%) mixed function. Powder X-ray diffraction (p-XRD) patterns of the samples were carried out on a D-8 Advance X-ray diffractometer (Bruker-AXS, Germany) using Cu Kα radiation (λ = 1.5406 Å) with a step size of 0.1° over a 2θ range from 5° to 80° with the electric current operated at 40 mA and the voltage being fixed at 40 kV. The pH of the point of

zero charge (pH_{pzc}) was identified by measuring the ζ-potential with a zeta potential analyzer (Nano Zetasizer 2000, Malvern Co., UK).

Batch adsorption experiments

Phosphate removal experiments by the materials were conducted at room temperature (25 ± 1°C) with the target phosphate concentration and an adsorbent dose of 0.5 g/L unless otherwise noted. Before the adsorbent was added, the pH of the solution was adjusted to the required values (± 0.2) and maintained at target pH values throughout the experiments by addition the NaOH or HCl solution (1 mol/L). After the addition of the adsorbents, the mixture suspensions were shaken in a thermostatic shaker at 180 rpm. Following the reaction period, samples were collected through a 0.22 μm membrane syringe filter for phosphate concentration analysis. The residual phosphate concentrations of the supernatant solutions were determined by a molybdenum-blue ascorbic acid method with a UV-Vis spectrophotometer at 880 nm (UV-2550, Shimadzu, Japan) (Chen et al. 2015). All experiments were repeated in triplicate, and the average values were used to analyze the results. The removal efficiency (*RE*) was determined as follows:

$$RE = \frac{C_0 - C_e}{C_0} \quad (1)$$

where the initial concentration of the phosphate solution is C_0 (mg/L) and the equilibrium concentration of the phosphate solution is C_e (mg/L), the volume of the phosphate solution is V (L) and the weight of the adsorbent used in the experiments is m (g).

The adsorption capacity of phosphate removed by the adsorbent (q_e, mg•g^{-1}) was calculated as the difference between the initial and residual phosphate concentrations in solution divided by the weight of the adsorbent as followed:

$$q_e = \frac{(C_0 - C_e) \times V}{m} \quad (2)$$

where C_0 and C_e are same as mentioned above, V is the volume of the phosphate solution (L) and m is the weight of the adsorbent (g).

Adsorption isotherms, adsorption kinetics and the effect of pH and coexisting anions were performed in order to evaluate the performance of phosphate adsorption by the adsorbents. The phosphate adsorption kinetics were carried out by adding 0.125 g of Fe-La binary (hydr)oxides to a 250 mL phosphate solution with an initial concentration of 50 mg/L at pH 4.0. Approximately 2 mL samples were taken out at predetermined times and filtered immediately. The adsorption isotherm experiments were investigated by adding 0.05 g of adsorbent into 100 mL of phosphate solutions with different initial concentrations

(30.0–80.0 mg•L^{-1}) at pH 4.0 for 24 h. The influence of solution pH on phosphate adsorption was measured by adding 0.05 g of Fe-La binary (hydr)oxides to phosphate solutions of 50 mg/L under the different pH values ranging from 3 to 11 for 24 h. To explore the effect of common coexisting anions, 0.05 g of Fe-La binary (hydr)oxides were added to 100 mL phosphate solutions (50 mg/L) in the presence and absence of NaCl, Na_2SO_4, $NaHCO_3$, and $NaCH_3COO$, respectively, and the initial concentrations of the coexisting anions were set in the range of 10–100 mmol•L^{-1}. Specially, the CH_3COO^- anion is a representative of natural organic acids (NOAs) in the tests. For the reusability study, adsorption and desorption experiments were carried out for four cycles at pH 7.0, and the desorption experiments were conducted over 4 h using 0.2 mol/L NaOH solution. The initial phosphate concentration was 50.0 mg/L, and the adsorbent dose was 0.5 g/L

Results And Discussion

Characterization of materials

Scanning electron microscopy

The surface morphologies and element distributions of the Fe-La binary (hydr)oxides before and after phosphate adsorption were characterized by SEM-EDX. As illustrated in Fig. 1a, SEM images show that the Fe/La 3:1 adsorbent has rough surfaces and consists of irregular and aggregated small particles with different sizes. Groups of aggregated blocks covered with granules were formed on the surface of the Fe/La 1:1 adsorbent (Fig. 1b). For the Fe/La 1:3 adsorbent, the grains were consisted of nanoflake aggregates and smaller particles of various sizes (Fig. 1c). With the decrease of the Fe/La ratios, an increasing number of morphologies and structures similar to those of pure La (hydr)oxide were observed on the surface of the adsorbents (Zhang et al. 2014). After phosphate adsorption, the surface of the adsorbents became rougher and more irregular, and needle-like nanocrystals were formed, as presented in Fig. 1d-1f. The needle-like nanocrystals corresponding to $CePO_4$ were also observed after phosphate adsorption by biochar-loaded Ce^{3+}-enriched ultra-fine ceria nanoparticles (Wang et al. 2020). There were no obvious discrepancies among the phosphate-loaded adsorbents with different Fe/La molar ratios. Furthermore, the EDX surface element analysis of the adsorbents after phosphate removal (Fig. 2) revealed that phosphate was successfully removed by the adsorbents. Furthermore, the contents of phosphate element on the surface were approximately 4.42 wt% for the Fe/La 3:1 adsorbent, 10.49 wt% for the Fe/La 1:1 adsorbent and 14.64 wt% for the Fe/La 1:3 adsorbent, indicating that the performance of phosphate adsorption was enhanced with the decrease of the Fe/La ratios. This result was further confirmed by the results of the batch adsorption experiments described below.

Specific surface area

The N_2 adsorption–desorption isotherms and the pore size distributions estimated by the BJH analysis using desorption data of the Fe-La binary (hydr)oxides are depicted in Fig. 3a. As shown in Fig. 3a, the adsorption–desorption isotherms of the Fe/La binary (hydr)oxides were attributed to the characteristics of type IV isotherms with H3-type hysteresis loops according to the IUPAC classification, suggesting that

the multilayered physical adsorption of N_2 occurred between the aggregates of the adsorbents. These results indicate that the materials were possibly mesoporous, as presented in Fig. 3a.

The specific surface areas, *t*-plot micropore areas, average pore diameters, and average pore volumes of Fe-La binary (hydr)oxides obtained from the N_2 adsorption–desorption isotherms are summarized in Table 1. It can be seen that the Fe/La 1:3 (hydr)oxides showed the highest specific surface area of 137.1 m^2/g, while the Fe/La 1:1 (hydr)oxides exhibited the lowest specific surface area of 16.3 m^2/g. For the *t*-plot micropore area and average pore volume, the Fe-La binary (hydr)oxides showed similar trends with changes in the Fe/La ratios. These observations indicated that the incorporation of Fe and La metals on the Fe/La 1:1 (hydr)oxides was different from that of the other two type Fe-La (hydr)oxides (Yu et al. 2019). However, the average pore diameters were 35.2, 103.3 and 192.8 Å for the Fe/La 3:1, Fe/La 1:1 and Fe/La 1:3 (hydr)oxides, respectively, and increased with the increase in La contents, which may be attributed to the change of the particle shape from irregular and aggregated particles to nanoflakes, as observed by SEM in Fig. 1.

Table 1
BET specific surface areas and porosity measurements of Fe-La binary (hydr)oxides.

Adsorbent	Specific surface area (m^2/g)	*t*-plot micropore area (m^2/g)	Average pore diameter (Å)	Average pore volume (cm^3/g)
Fe/La 3:1	137.1	4.75	35.2	0.133
Fe/La 1:1	16.3	2.18	103.3	0.061
Fe/La 1:3	81.1	4.22	192.8	0.487

Point of zero charge

The surface zeta potentials of the adsorbents at different pH values are presented in Fig. 3b. It can be observed that the pH_{pzc} values of Fe/La 3:1, Fe/La 1:1 and Fe/La 1:3 (hydr)oxides were found to be about 7.92, 8.49 and 9.37, respectively. Obviously, the pH_{pzc} value raised with the increase of La contents. Previous researches demonstrated that the pH_{pzc} of ferrihydrite was pH 7–9 (Masue et al. 2007), and that the pH_{pzc} of lanthanum hydroxide was pH 9–10.5 (Xu et al. 2017, Zhang et al. 2014). The surface charge of the adsorbent is highly affected by solution pH. When the pH value of the solution is below their pH_{pzc}, positive charges would be formed on the surface of the adsorbent, and the stronger electrostatic attraction between active sites of the adsorbent and phosphate is favorable for the efficient phosphate removal. On the other hand, the surface of the adsorbent is negatively charged when $pH > pH_{pzc}$, which is not conducive to the uptake of phosphate due to the enhancement of electrostatic repulsion.

Batch adsorption experiments

Adsorption kinetics

In order to estimate the rate of phosphate removal, the amounts of phosphate adsorbed onto Fe-La binary (hydr)oxides as a function of contact time were conducted at pH 4.0 with an initial phosphate concentration of 50.0 mg/L and the results are shown in Fig. 4a. It is clearly that the adsorption rates were rapid within the first 6 h, and thereafter followed by a relatively slow adsorption step. Approximately 67.6%, 87.9% and 100% of the equilibrium adsorption capacities of Fe/La 3:1, Fe/La 1:1 and Fe/La 1:3 binary (hydr)oxides were achieved within the first 6 h, respectively. It should be noted that nearly 99.3% of the total phosphate contents had been removed by the Fe/La 1:3 (hydr)oxides after 1.5 h of reaction. The initial rapid adsorption behavior might be attributed to the large amounts of unoccupied and freely available adsorption sites, which was favorable for the transportation of phosphate onto the surface of the adsorbents. With the decrease in the number of vacant sites, surface precipitation and intraparticle diffusion were the dominant mechanisms of phosphate adsorption, and the adsorption rate was slow (Lu et al. 2013, Zhang et al. 2016).

The kinetic data of phosphate adsorption were fitted using pseudo-first-order model and pseudo-second-order models in order to further understand the characteristics of the adsorption process. These two models can be expressed as:

$$\ln(q_e - q_t) = \ln q_e - k_1 t \quad (3)$$

$$\frac{t}{q_t} = \frac{1}{k_2 q_e^{\,2}} + \frac{t}{q_e} \quad (4)$$

where q_e (mg/g) and q_t (mg/g) represent the amounts of phosphate adsorbed at time t and at equilibrium, respectively, and k_1 (h^{-1}) and k_2 (g/(mg•h)) are the rate constants of the pseudo-first-order and pseudo-second-order models, respectively.

The fitting parameters estimated from the kinetic models are represented in Table 2. It is obvious that the experimental data were described better by the pseudo-second-order equation model with higher values of correlation coefficient ($R^2 > 0.99$) being observed. This indicates that the dominant adsorption process could be attributed to chemisorption or chemical bonding between the active sites of the adsorbents and phosphate. In addition, the calculated k_2 values of phosphate removal derived from the pseudo-second-order equation model for Fe/La 3:1, Fe/La 1:1 and Fe/La 1:3 binary (hydr)oxides were 0.0084, 0.0162 and 0.0333 g/(mg•h), respectively, indicating that the increase of the La contents in Fe-La binary (hydr)oxides not only increased the adsorption capacity at equilibrium, but also enhanced the adsorption rate.

Table 2
Adsorption kinetic parameters for phosphate adsorption onto Fe/La 3:1, Fe/La 1:1 and Fe/La 1:3 binary (hydr)oxides.

Adsorbent	Pseudo-first-order kinetic model			Pseudo second-order kinetic model		
	q_e (mg/g)	k_1 (h^{-1})	R^2	q_e (mg/g)	k_2 (g/(mg•h))	R^2
Fe/La 3:1	42.72	0.2639	0.9676	47.62	0.0084	0.9959
Fe/La 1:1	59.87	0.9534	0.8673	66.23	0.0162	0.9963
Fe/La 1:3	98.92	7.081	0.9526	100.0	0.0333	0.9982

Adsorption isotherms

In order to evaluate the phosphate adsorption capacities, the adsorption isotherm experiments for phosphate onto Fe-La binary (hydr)oxides were performed at pH 4.0 ± 0.2 with different initial concentrations ranging from 30 to 80 mg•L^{-1}. The obtained isotherms are depicted in Fig. 4b. It is seen that the amount of phosphate uptake increased as the initial concentration increased, and that the adsorption capacity increased significantly with the decrease of the Fe/La molar ratios. Both Langmuir and Freundlich adsorption isotherm models were employed to quantitatively describe the experimental data. The Langmuir and Freundlich isotherm models can be represented as follows (Wang et al. 2016, Wang et al. 2020, Zhang et al. 2021):

$$\frac{C_e}{q_e} = \frac{1}{q_{max}} C_e + \frac{1}{K_L q_{max}} \quad (5)$$

$$\log q_e = \log K_F + \frac{1}{n} \log C_e \quad (6)$$

where C_e (mg/L) is the equilibrium concentration of phosphate, q_e (mg/g) and q_m (mg/g) are the equilibrium and maximum adsorption capacities, respectively, K_L (L/mg) and K_F (mg/g) are the adsorption constants for the Langmuir and Freundlich models, respectively, which could be used to roughly represent the affinity of phosphate adsorption. 1/n is a heterogeneity factor related to the adsorption intensity.

The adsorption isotherm fitting curves are shown in Fig. 4b and the parameters acquired from the Langmuir and Freundlich adsorption isotherm models are listed in Table 3. As illustrated in Table 3, it can be found that the higher regression coefficients (R2 > 0.99) of the Langmuir model suggested that the Langmuir model fitted the isotherm data better than the Freundlich model, indicating that the adsorption of phosphate on Fe-La binary (hydr)oxides was likely a process of monolayer adsorption and that the adsorbed sites were homogeneously distributed on the surface of the adsorbents (Liu et al. 2019, Wang

et al. 2020). The maximum phosphate adsorption capacities of Fe/La 3:1, Fe/La 1:1 and Fe/La 1:3 binary (hydr)oxides calculated from the Langmuir model were 49.02, 69.44 and 136.99 mg/g, respectively, which suggested that higher La contents in Fe-La binary (hydr)oxides would result in greater ability of phosphate removal. Specially, Yu et al. proposed a new strategy for the development of materials by activation of lattice oxygen in binary (hydr)oxides, and a LaFe (oxy)hydroxide (FL2:1) adsorbent showed that the maximum phosphate adsorption capacity of the adsorbent was 123.46 mg/g, which is lower than that of the Fe/La 1:3 binary (hydr)oxides (Yu et al. 2019).

Moreover, Table 4 summaries compared the maximum adsorption capacities of the Fe-La binary (hydr)oxides from this study with those of some other La-based adsorbents previously reported. As illustrated in Table 4, the Fe-La binary (hydr)oxides shows much better performance than most of the previously reported adsorbents, indicating their specific potential for phosphate removal.

Table 3
Langmuir and Freundlich isotherm parameters for phosphate adsorption on Fe/La 3:1, Fe/La 1:1 and Fe/La 1:3 binary (hydr)oxides.

	Langmuir model			**Freundlich model**		
	q_{max} (mg/g)	k_L (L/mg)	R^2	n	k_F (mg/g)	R^2
Fe/La 3:1	49.02	0.1981	0.9771	7.407	26.65	0.6971
Fe/La 1:1	69.44	1.043	0.9947	32.41	59.46	0.7575
Fe/La 1:3	136.99	1.197	0.9978	23.34	113.83	0.7786

Table 4
Comparison of the maximum phosphate adsorption capacities of various La-based sorbents.

Adsorbent	pH	q_{max} (mg/g)	Ref.
$La(OH)_3/Fe_3O_4$ (4:1)	7.0	83.5	(Wu et al. 2017)
$Fe_3O_4@SiO_2@La_2O_3$	6.59	27.8	(Lai et al. 2016)
FMS-0.2La	n.a.	44.82	(Huang et al. 2015)
La_{100}SBA-15	n.a.	45.6	(Yang et al. 2011)
La-BC-5	3.0	23.52	(Xu et al. 2020)
LAH-1/10	4.0	128.2	(Xu et al. 2017)
La_3-MPBC	6.0	116.08	(Zhang et al. 2021)
La-201	6 – 7	57.4	(Zhang et al. 2016)
Lanthanum hydroxide nanorods	7.0	170.1	(Fang et al. 2017)
NiLa-LDOs/Fe_3O_4	7.0	203.10	(Vu &Wu 2020)
LaFe (oxy)hydroxide (FL2:1)	7.0	123.46	(Yu et al. 2019)
Fe/La 1:3	4.0	136.99	This study
Note: n.a.: not available.			

Effect of pH on phosphate removal

Solution pH is one of the most important factors in phosphate removal because it can affect both the surface charge of adsorbents (Fig. 3b) and phosphate species (**Fig. S1**). Herein, the effect of solution pH on phosphate removal by Fe-La binary (hydr)oxides was investigated in the pH range of 3–11 with an initial phosphate concentration of 50 mg/L and the results are presented in Fig. 4c. Apparently, the uptake of phosphate by the Fe-La binary (hydr)oxides was remarkably dependent on solution pH. The greatest degree of adsorption was observed under acidic conditions, and the removal efficiency reduced dramatically with the increase of solution pH. The decline of phosphate adsorption capacity with the increase of pH has also been reported in previous literatures (Lu et al. 2013, Wang et al. 2020, Zhang et al. 2021). However, this trend is significantly distinct with that by $La(OH)_3/Fe_3O_4$ nanocomposite, by which the highest level of phosphate removal was observed between pH 4.3 and 6 (Wu et al. 2017). This discrepancy might be due to the formation of surface co-precipitation of lanthanum phosphate under acidic conditions (Fang et al. 2017, Yu et al. 2019, Zhang et al. 2016). Furthermore, the phosphate capacity of Fe-La binary (hydr)oxides increased with the decrease of the Fe/La molar ratios with respect to the same pH value. This observation was similar to those of adsorption kinetics (Fig. 4a) and adsorption isotherms (Fig. 4b), and was further confirmed by EDX surface elemental analysis (Fig. 2).

As given in **Fig. S1**, monovalent $H_2PO_4^-$ was the main species of phosphate in the pH range of 3–6, and the surfaces of the adsorbents were fully protonated. The decrease of pH was favourable for protonation. Consequently, the positively charged adsorbents could effectively interact with the negatively charged $H_2PO_4^-$ through electrostatic attractions, thus leading to the enhanced phosphate sorption capacity under acidic conditions. With the increase in solution pH, divalent HPO_4^{2-} became the dominant species in the pH range of 7–11, and the surfaces of the adsorbents were deprotonated. The surface charge of the adsorbents could become negative when the pH value of the solution was above the pH_{pzc} of the adsorbent. The negatively charged adsorption sites and the negatively charged HPO_4^{2-} gradually promoted the electrostatic repulsion, which would be unfavourable for phosphate removal. What's more, the lower affinity of the surface of $La(OH)_3$ for HPO_4^{2-} compared to that for $H_2PO_4^-$ due to the hydroxylation of lanthanum ions also resulted into the sharply decrease of the phosphate removal under alkaline conditions (Wu et al. 2017, Zhang et al. 2021).

In addition, the release of La and Fe in solution after phosphate adsorption at different pH values was evaluated as shown in **Fig. S2**. The leaching of Fe was not detected in the experiments. However, the release of La was found under acidic conditions and can be negligible at pH > 5. The concentrations of La release in solution at pH 3.0 were found to be 0.22, 1.56 and 18.98 mg/L for the Fe/La 3:1, Fe/La 1:1 and Fe/La 1:3 binary (hydr)oxides, respectively, indicating that the increase of La contents in Fe-La binary (hydr)oxides could promote the dissolution of La. The release of La in solution has also been observed by other La-based sorbents, such as nano-La(III) (hydr)oxides modified-wheat straw (Qiu et al. 2017), $La(OH)_3/Fe_3O_4$ nanocomposite (Wu et al. 2017) and magnetic porous biochar supported $La(OH)_3$ (Zhang et al. 2021). Therefore, a rather low solubility product constant ($K_{sp} = 3.7 \times 10^{-23}$) suggests that the insoluble lanthanum phosphate ($LaPO_4$) precipitation was formed under acidic conditions, which was further discussed as below.

Regeneration and reusability

To estimate the reusability of the Fe-La binary (hydr)oxides, their regeneration using 0.2 mol/L NaOH solution and re-adsorption were performed. Four reusability cycles were carried out, and the results were depicted in Fig. 4d. The adsorption capacities of cycle 0 correspond to those of the origin adsorbents. Apparently, the adsorption capacities of the adsorbents significantly decreased after the first cycle and exhibited the lower and more stable adsorption capacities after two cycles, which could be attributed to the formation of the insoluble lanthanum phosphate ($LaPO_4$) co-precipitation.

Effect of co-existing anions

Environmental phosphate always coexists with various anions in natural water environments or industrial effluents. The presence of competitive anions may interfere with phosphate adsorption. In this study, the effects of Cl^-, SO_4^{2-}, HCO_3^-, and acetate (Ac^-), as a representative of NOAs, on phosphate removal by the Fe-La binary (hydr)oxides were investigated at pH 7.0 with an initial phosphate concentration of 50.0

mg/L. As presented in Fig. 5, it is obvious that the uptake of phosphate was negligibly affected by the presence of Cl^-, and SO_4^{2-}, even at concentrations of up to 100 mmol/L. however, there was slight interference from HCO_3^-, and acetate. Similar effects with respect to these competing ions on phosphate removal have been reported in previous studies (Fang et al. 2017, Wang et al. 2020, Wu et al. 2017).

Analysis of Fe-La binary (hydr)oxides before and after phosphate adsorption

In view of the above experimental results, a series of analytical techniques, including p-XRD, FTIR and XPS, were employed to characterize the Fe-La binary (hydr)oxides before and after phosphate adsorption in order to further investigate the mechanisms of phosphate removal.

XRD analysis

p-XRD spectra were used to elucidate the phase compositions of the Fe-La binary (hydr)oxides before and after phosphate adsorption. Figure 6a presents the p-XRD patterns of these materials, which are in comparison with the patterns of the synthesized lanthanum hydroxide ($La(OH)_3$) and a model compound of rhabdophane ($LaPO_4•0.5H_2O$, JCPDS 46 − 1439). The XRD pattern of Fe/La 3:1 (hydr)oxides shows diffraction peaks with 2θ values identified at 23.7°, 33.5° and 41.4°, which can be assigned to the crystal planes of bemalite ($Fe(OH)_3•0.25H_2O$, JCPDS 81 − 2022). Diffraction peaks with 2θ values at 26.4°, 29.3° and 46.2° and these with 2θ values at 37.8° and 444.6° can be attributed to different phases of La_2O_3 for JCPDS 83 − 1344 and JCPDS 83 − 1349, respectively. Diffraction peaks attributed to the phase of hexagonal [P63/m (no.176)] lanthanum hydroxide ($La(OH)_3$, JCPDS 83 − 2034) were observed at 2θ values of 15.6° and 48.4°. For the Fe/La 1:3 (hydr)oxides, only broad diffraction peaks belonging to the phase of La_2O_3 and $La(OH)_3$ could be observed, which indicates that the particle size of the nanocrystals was very small and/or the crystallinity was poor. After phosphate adsorption, all peaks assigned to the virgin binary (hydr)oxides disappeared. Peaks appearing at 2θ values of 14.1°, 19.9°, 25.1°, 29.1°, 31.1°, 41.2° and 48.2° were broad, which can be indexed to the hexagonal phase of rhabdophane ($LaPO_4•0.5H_2O$, JCPDS 46 − 1439). Furthermore, their intensities were low, indicating that the newly formed rhabdophane was amorphous and that the crystal structures of the Fe-La binary (hydr)oxides were destroyed due to the interaction between phosphate and Fe-La binary (hydr)oxides. These results reveal that the formation of rhabdophane was the main mechanism of phosphate removal.

FTIR analysis

FTIR spectra of the Fe-La binary (hydr)oxides before and after phosphate adsorption are depicted in **Fig. S3**. As illustrated in **Fig. S3**, it is common sense for us that broad vibration bands located at 3433 and 1634 cm^{-1} are observed for all materials, which can be ascribed to the stretching vibration of adsorbed water molecules and the bending vibration of the —OH group, respectively (Wang et al. 2020, Yu et al. 2019). As shown in Fig. 6b, peaks of pristine (oxy)hydroxides located at 462 cm^{-1} correspond to the stretching of Fe − O bonds, and weak band appearing at 1050 cm^{-1} can be attributed to the bending

vibrations of La – OH bonds (Li et al. 2012, Zhang et al. 2012). Peaks centered at 1388 cm^{-1} are assigned to the vibration mode of NO_3^- anions due to the residues from the raw synthetic materials of $La(NO_3)_3•6H_2O$ according to the previous literatures (Li et al. 2012), and its intensity significantly decreased after phosphate removal. However, Zhang et al. demonstrated that the vibration bands at 1490 cm^{-1} and 1394 cm^{-1} were the characteristics of the lanthanum (hydr)oxide (Zhang et al. 2014). Furthermore, these peaks have also been reported by other binary (hydr)oxides, such as Mn–La composites (Yu &Chen 2014). Therefore, the attribution of the peaks at 1480 cm^{-1} and 1388 cm^{-1} needs further research. After phosphate adsorption, new strong vibration bands at 1055 cm^{-1} and new shoulder vibration bands at 1018 cm^{-1} are observed and can be respectively assigned to the asymmetric and the symmetric stretching vibrations of P – O bonds, respectively. Two other new peaks appeare at 617 cm^{-1} and 538 cm^{-1}, which belonged to the bending vibrations of O – P bonds (Wang et al. 2020). The FTIR results suggest that chemical interactions between phosphate and the Fe-La binary (hydr)oxides occurred, resulting in the formation of inner-sphere complexes (Chen et al. 2019).

XPS analysis

X-ray Photoelectron Spectroscopy is considered as a powerful technique for the characterization of the surface electronic structure and bonding configuration of materials. As illustrated in Fig. 7a, the wide scan XPS spectra of the pristine Fe-La binary (hydr)oxides indicate that Fe, La and O are present in the composites. After phosphate adsorption, the appearance of the P 2p characteristic peak at ~ 133.8 eV demonstrates the successful loading of phosphate on La-Fe binary hydroxides. Figure 7b and 7c present the XPS spectra of La 3d and Fe 2p before and after phosphate adsorption, respectively. The XPS spectra of La 3d are mainly consist of La $3d_{5/2}$ and La $3d_{3/2}$ due to the spin-orbit splitting (Yu et al. 2015). The representative peaks of La 3d located at ~ 835.1 and ~ 839.0 eV and those centered at ~ 852.2 and ~ 855.9 eV can be assigned to La $3d_{5/2}$ and La $3d_{3/2}$, respectively (Yu et al. 2019, Yu &Chen 2014). The typical peak positions of Fe 2p appear at ~ 711.0 eV for Fe $2p_{3/2}$ and ~ 724.3 eV for Fe $2p_{1/2}$. The binding energies corresponding to the peaks of La 3d and Fe 2p of the Fe/La 1:1 (hydr)oxides exhibited no obvious change after phosphate adsorption. However, the binding energies corresponding to the peaks of La 3d shifted to lower values with the increase of La contents, and to higher values with the decrease of La contents. In contrast, the binding energies corresponding to the peaks of Fe 2p shifted to higher values with the increase of Fe contents, and to lower values with the decrease of Fe contents. These discrepancies in the change of the binding energies as the variety of the metal composition indicate that the electronic migration between La and P due to the adsorption could be different from that between Fe and P. These divergences further resulted in irregular energy changes in the binding energies corresponding to the peaks of P 2p, which were located at 133.4 eV for the Fe/La 3:1 (hydr)oxides, 134.4 eV for the Fe/La 1:1 (hydr)oxides and 133.8 eV for the Fe/La 1:3 (hydr)oxides (Fig. 7d).

The high resolution scans of O 1s spectra of the Fe-La binary (hydr)oxides before and after phosphate adsorption were employed to further investigate the mechanisms of phosphate adsorption. As depicted in Fig. 8, the binding energies corresponding to the peaks of O 1s after phosphate removal shifted from

530.8 eV to 531.4 eV for the Fe/La 3:1 (hydr)oxides, from 532.0 eV to 531.7 eV for the Fe/La 1:1 (hydr)oxides and from 531.7 eV to 531.0 eV for the Fe/La 1:3 (hydr)oxides. The broad and asymmetric O 1s peaks in the XPS spectra of the original (hydr)oxides likely correspond to two chemical states of O: metal oxides (M–O) and hydroxyl groups bonded to the metal (M–OH). After phosphate adsorption, a new component peak appeared, which could be identified as phosphate oxygen (P–O). The relative area ratio for the peak attributed to M–OH decreased from 50.5–27.8% for the Fe/La 3:1 (hydr)oxides, from 66.5–28.9% for the Fe/La 1:1 (hydr)oxides and from 61.3–32.1% for the Fe/La 1:3 (hydr)oxides after phosphate removal, indicating that phosphate was adsorbed onto Fe-La (hydr)oxides through surface hydroxyl exchange reactions. This phenomenon was also observed in previous studies on phosphate and/or arsenic removal (Lu et al. 2013, Yu et al. 2015, Yu et al. 2017).

Removal mechanisms

Based on the above analysis, the main mechanisms of phosphate removal by Fe-La binary (hydr)oxides are proposed to be based on the formation of rhabdophane through surface hydroxyl exchange reactions and co-precipitation of La^{3+} and phosphate ions. Surface hydroxyl exchange reactions were the predominate adsorption mechanisms and can be described as following (where ≡ S represents the surface):

$$2[\equiv S-OH_2^+]\,(s) + (HO)_2PO_2^- \rightarrow (\equiv S-O-)_2P-(OH)_2 + H_2O \qquad (7)$$

Under acidic and neutral conditions, $H_2PO_4^-$ is the predominant species in solution, and La^{3+} ions were released into solution. In addition to surface hydroxyl exchange reactions, co-precipitation of released La^{3+} and phosphate ions led to the formation of insoluble rhabdophane as following:

$$La^{3+} + H_2PO_4^- \rightarrow LaPO_4 \qquad (8)$$

Under alkaline conditions, the release of La decreased dramatically, and surface hydroxyl exchange reactions became the main removal mechanisms, resulting into a sharp reduction in removal efficiency with the increase of solution pH.

Conclusions

In summary, Fe-La binary (hydr)oxides were prepared by a co-precipitation method and their performances of phosphate removal were studied. The binary (hydr)oxides exhibited excellent performances in phosphate removal. The adsorption capacity of phosphate increased with the increase of La contents, and the calculated Langmuir capacities of Fe/La 3:1, Fe/La 1:1 and Fe/La 1:3 binary (hydr)oxides at pH 4.0 were 49.02, 69.44 and 136.99 mg/g, respectively. The removal efficiency was remarkably dependent on solution pH and significantly reduced with the increase of pH. Based on the

analyses of p-XRD, FTIR and XPS, the formation of amorphous rhabdophane phase through surface hydroxyl exchange reactions and co-precipitation of released La^{3+} and phosphate ions were the dominant removal mechanisms. The high removal efficiencies of Fe-La binary (hydr)oxides indicates their specific potential on the treatment of P-contaminated water.

Declarations

Funding information

The authors are grateful to the National Natural Science Foundation of China (No. 41807358) and the Joint Fund of NSFC and Henan (No. U1804110).

Electronic supplementary material

Supplementary material associated with this article can be found, in the online version, at doi: http://dx.doi.org/XXXXXXXXXX, which is available to authorized users.

Authors' contributions

Haijing Duan: Investigation, Writing - original draft. **Lin Zhang**: Investigation. **Yulong Wang**: Conceptualization, Methodology, Writing - review & editing, Supervision, Funding acquisition. **Yanhong Liu**: Formal analysis, Investigation, Writing - review & editing, Supervision. **Yangyang Wang**: Writing – review, Supervision, Funding acquisition. all the authors participated in the revision of the manuscript.

Data availability and materials

All the materials and data in this study can be found in this paper

Compliance with ethical standards

Conflict of interest

The authors declare that they have no financial or personal relationship with any other person or organization that may unduly affect our work, and they have no known competing financial interests or personal relationships that could have appeared to influence the word reported in this paper.

Ethical Approval

The authors declare that they have no known competing financial interests or personal relationships that could have appeared to influence the word reported in this paper.

Consent to participate

All the authors volunteered to participate in this study.

Consent to publish

All the authors agreed to publish the manuscript.

References

Chen L, Li Y, Sun Y, Chen Y, Qian J (2019) $La(OH)_3$ loaded magnetic mesoporous nanospheres with highly efficient phosphate removal properties and superior pH stability. Chem Eng J 360:342-348

Chen ML, Huo CB, Li YK, Wang JH (2015) Selective adsorption and efficient removal of phosphate from aqueous medium with graphene-lanthanum composite. Acs Sus Chem Engin 4(3):1296-1302

Conley DJ, Paerl HW, Howarth RW, Boesch DF, Seitzinger SP, Havens KE, Lancelot C, Likens GE (2009) ECOLOGY controlling eutrophication: nitrogen and phosphorus. Science 323(5917):1014-1015

Dithmer L, Lipton AS, Reitzel K, Warner TE, Lundberg D, Nielsen UG (2015) Characterization of phosphate sequestration by a lanthanum modified bentonite clay: a solid-state NMR, EXAFS, and PXRD study. Environ Sci Technol 49(7):4559-4566

Fang L, Shi Q, Nguyen J, Wu B, Wang Z, Lo IMC (2017) Removal mechanisms of phosphate by lanthanum hydroxide nanorods: investigations using EXAFS, ATR-FTIR, DFT, and surface complexation modeling approaches. Environ Sci Technol 51(21):12377-12384

Huang W, Zhu Y, Tang J, Yu X, Zhang Y (2014) Lanthanum-doped ordered mesoporous hollow silica spheres as novel adsorbents for efficient phosphate removal. J Mater Chem A 2(23):8839-8848

Huang W, Yu X, Tang J, Zhu Y, Zhang Y, Li D (2015) Enhanced adsorption of phosphate by flower-like mesoporous silica spheres loaded with lanthanum. Micropor Mesopor Mat 217:225-232

Lai L, Xie Q, Chi L, Gu W, Wu D (2016) Adsorption of phosphate from water by easily separable Fe_3O_4@SiO_2 core/shell magnetic nanoparticles functionalized with hydrous lanthanum oxide. J Colloid Interf. Sci 465:76-82

Li RH, Li Q, Gao S, Shang JK (2012) Exceptional arsenic adsorption performance of hydrous cerium oxide nanoparticles: Part A. Adsorption capacity and mechanism. Chem Eng J 185:127-135

Liu R, Chi L, Wang X, Wang Y, Sui Y, Xie T, Arandiyan H (2019) Effective and selective adsorption of phosphate from aqueous solution via trivalent-metals-based amino-MIL-101 MOFs. Chem Eng J 357:159-168

Lu J, Liu H, Liu R, Zhao X, Sun L, Qu J (2013) Adsorptive removal of phosphate by a nanostructured Fe-Al-Mn trimetal oxide adsorbent. Powder Technol 233:146-154

Masue Y, Loeppert RH, Kramer TA (2007) Arsenate and arsenite adsorption and desorption behavior on coprecipitated aluminum : iron hydroxides. Environ Sci Technol 41(3):837-842

Pan S, Zhang X, Wang Y, Liu J, Pan B (2020) Mesoporous polyacrylonitrile membrane with ultrahigh loading of well -dispersed Fe_2O_3 nanoparticles: a powerful phosphate scavenger enabling inhibition of microbial regrowth in treated water. J Membr Sci 603:118048

Qiu H, Liang C, Yu JH, Zhang QR, Song MX, Chen FH (2017) Preferable phosphate sequestration by nano-La(III) (hydr)oxides modified wheat straw with excellent properties in regeneration. Chem Eng J 315:345-354

Qu J, Akindolie MS, Feng Y, Jiang Z, Zhang G, Jiang Q, Deng F, Cao B, Zhang Y (2020) One-pot hydrothermal synthesis of $NaLa(CO_3)_2$ decorated magnetic biochar for efficient phosphate removal from water: Kinetics, isotherms, thermodynamics, mechanisms and reusability exploration. Chem Eng J 394:124915

Vu CT, Wu T (2020) Magnetic porous NiLa-Layered double oxides (LDOs) with improved phosphate adsorption and antibacterial activity for treatment of secondary effluent. Water Res 175:115679

Wang W, Ma C, Zhang Y, Yang S, Shao Y, Wang X (2016) Phosphate adsorption performance of a novel filter substrate made from drinking water treatment residuals. J Environ Sci 45:191-199

Wang Y, Xie X, Chen X, Huang C, Yang S (2020) Biochar-loaded Ce^{3+}-enriched ultra-fine ceria nanoparticles for phosphate adsorption. J Hazard Mater 396:122626

Wu B, Fang L, Fortner JD, Guan X, Lo IMC (2017) Highly efficient and selective phosphate removal from wastewater by magnetically recoverable $La(OH)_3/Fe_3O_4$ nanocomposites. Water Res 126:179-188

Xu R, Zhang M, Mortimer RJG, Pan G (2017) Enhanced phosphorus locking by novel lanthanum/aluminum-hydroxide composite: implications for eutrophication control. Environ Sci Technol 51(6):3418-3425

Xu X, Cheng Y, Wu X, Fan P, Song R (2020) La(III)-bentonite/chitosan composite: a new type adsorbent for rapid removal of phosphate from water bodies. Appl Clay Sci 190:105547

Yang J, Zhou L, Zhao L, Zhang H, Yin J, Wei G, Qian K, Wang Y, Yu C (2011) A designed nanoporous material for phosphate removal with high efficiency. J Mater Chem 21(8):2489-2494

Yu J, Xiang C, Zhang G, Wang H, Ji Q, Qu J (2019) Activation of lattice oxygen in LaFe (oxy)hydroxides for efficient phosphorus removal. Environ Sci Technol 53(15):9073-9080

Yu L, Ma Y, Ong CN, Xie J, Liu Y (2015) Rapid adsorption removal of arsenate by hydrous cerium oxide-graphene composite. RSC Adv 5(80):64983-64990

Yu Y, Chen JP (2014) Fabrication and performance of a Mn-La metal composite for remarkable decontamination of fluoride. J Mater Chem A 2(21):8086-8093

Yu Y, Zhang C, Yang L, Paul Chen J (2017) Cerium oxide modified activated carbon as an efficient and effective adsorbent for rapid uptake of arsenate and arsenite: Material development and study of performance and mechanisms. Chem Eng J 315:630-638

Zhang G, Liu H, Liu R, Qu J (2009) Removal of phosphate from water by a Fe-Mn binary oxide adsorbent. J Colloid Interf. Sci 335(2):168-174

Zhang L, Zhou Q, Liu J, Chang N, Wan L, Chen J (2012) Phosphate adsorption on lanthanum hydroxide-doped activated carbon fiber. Chem Eng J 185-186:160-167

Zhang W, Fu J, Zhang G, Zhang X (2014) Enhanced arsenate removal by novel Fe-La composite (hydr)oxides synthesized via coprecipitation. Chem Eng J 251:69-79

Zhang Y, Pan B, Shan C, Gao X (2016) Enhanced phosphate removal by nanosized hydrated La(III) oxide confined in cross-linked polystyrene networks. Environ Sci Technol 50(3):1447-1454

Zhang Y, Akindolie MS, Tian X, Wu B, Hu Q, Jiang Z, Wang L, Tao Y, Cao B, Qu JH (2021) Enhanced phosphate scavenging with effective recovery by magnetic porous biochar supported $La(OH)_3$: Kinetics, isotherms, mechanisms and applications for water and real wastewater. Bioresour Technol 319:124232

Figures

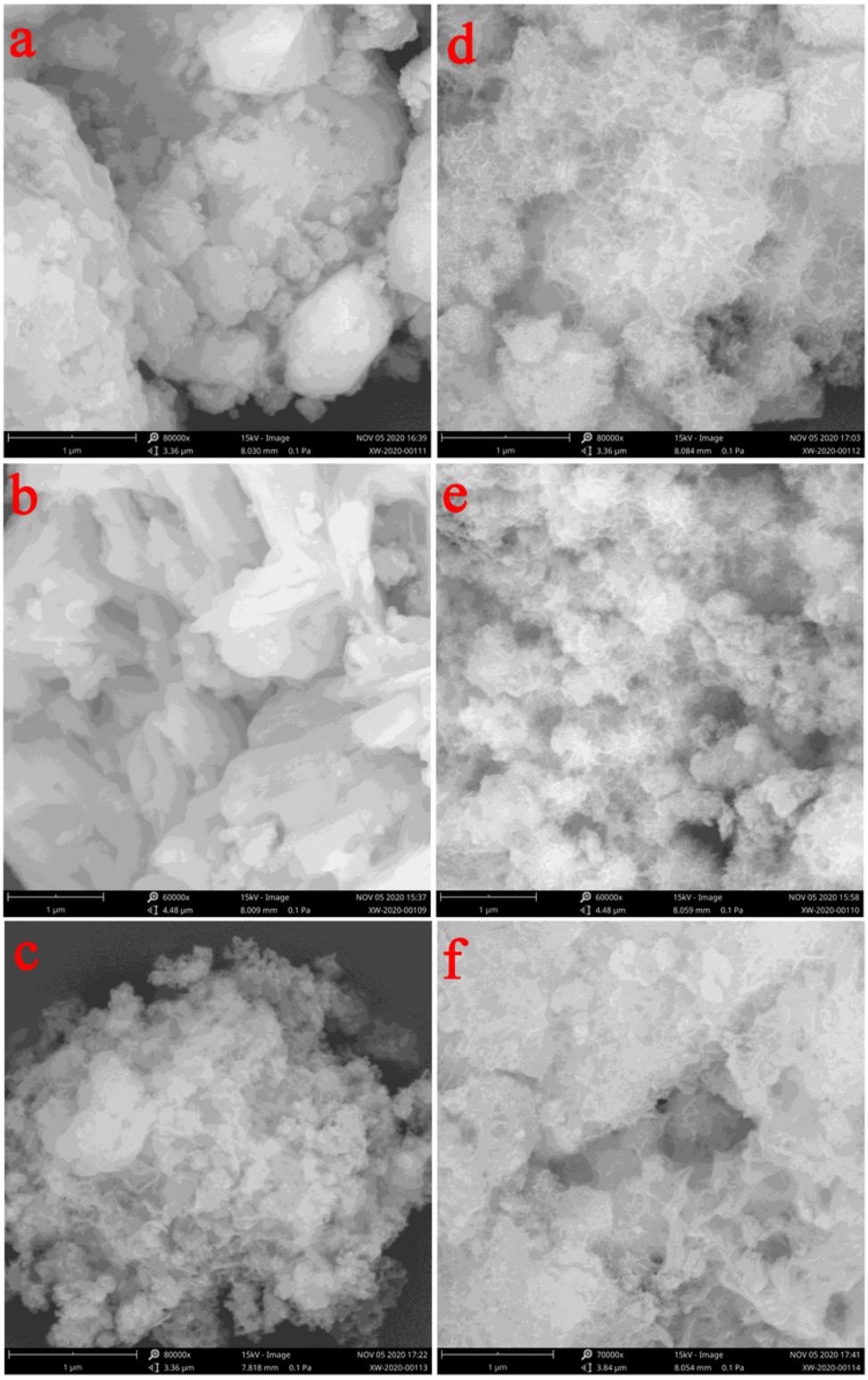

Figure 1

Surface morphologies of Fe/La 3:1 (hydr)oxides before (a) and after (d) phosphate adsorption, Fe/La 1:1 (hydr)oxides before (b) and after (e) phosphate adsorption and Fe/La 1:3 (hydr)oxides before (c) and after (f) phosphate adsorption.

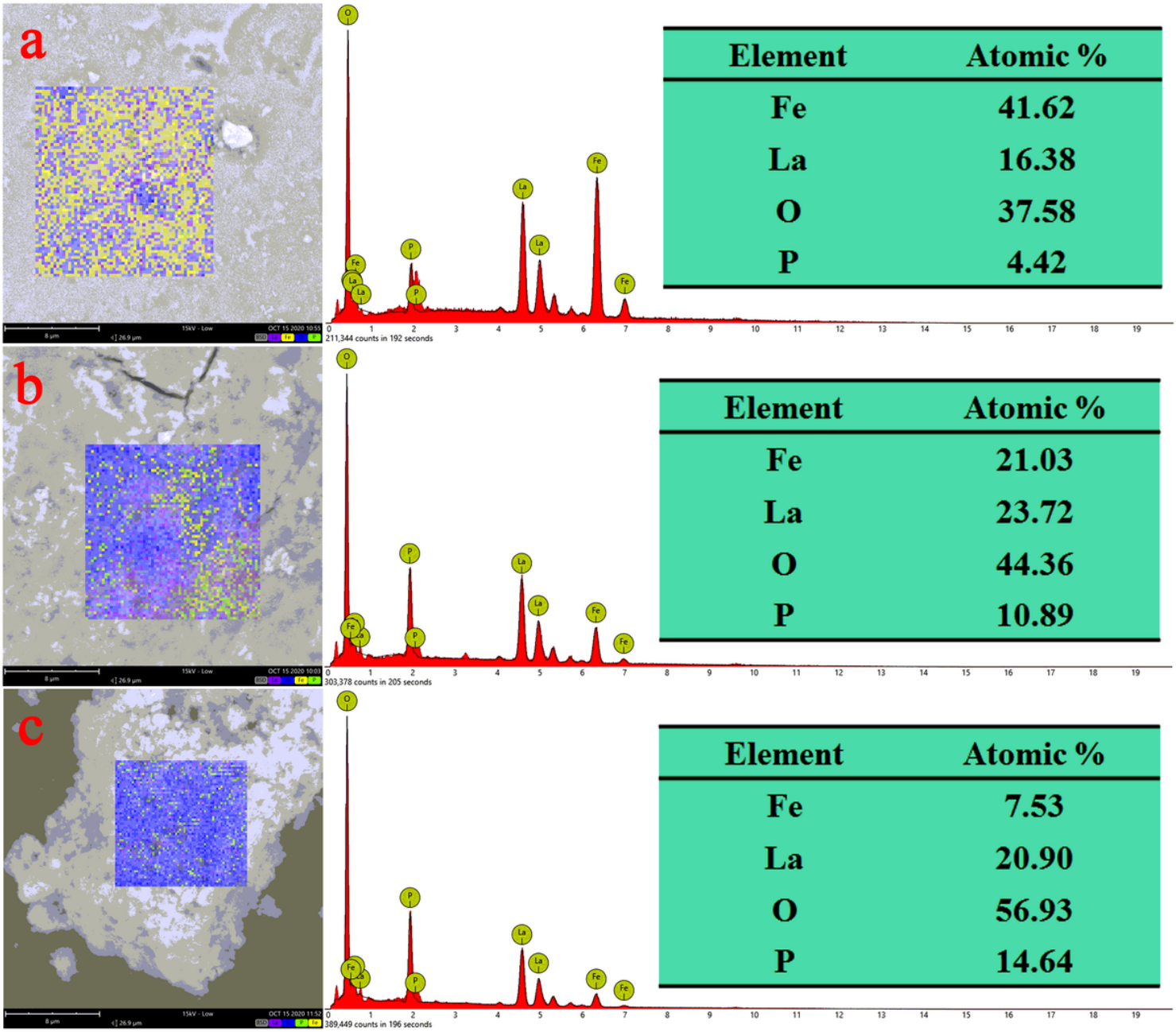

Figure 2

EDX analysis of Fe/La 3:1 (a), Fe/La 1:1 (b) and Fe/La 1:3 (c) binary (hydr)oxides after phosphate adsorption.

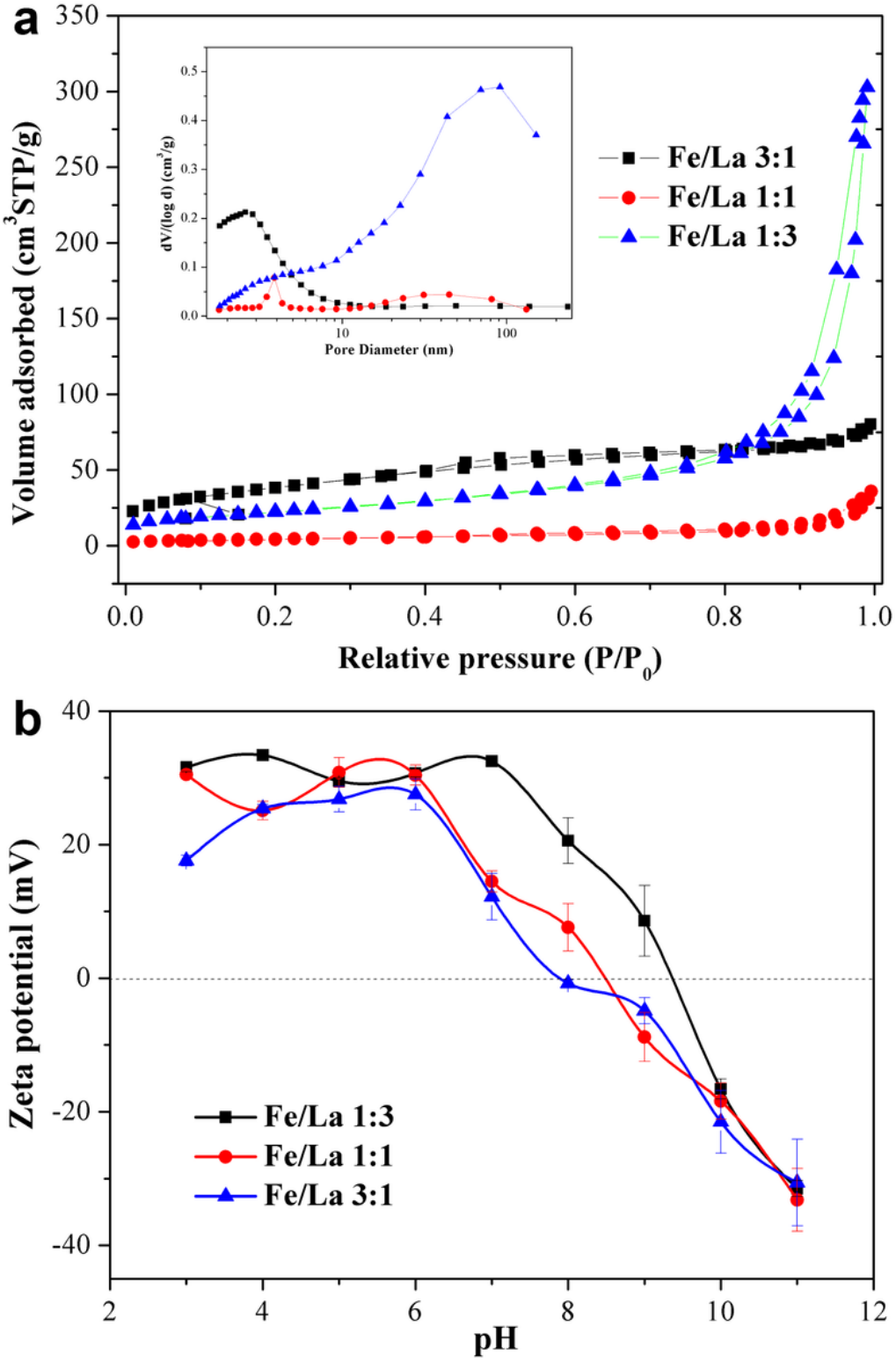

Figure 3

N2 adsorption–desorption isotherms and pore size distributions (inset) based on BJH analysis (a) and zeta potentials as a function of pH (b) of Fe/La 3:1, Fe/La 1:1 and Fe/La 1:3 binary (hydr)oxides.

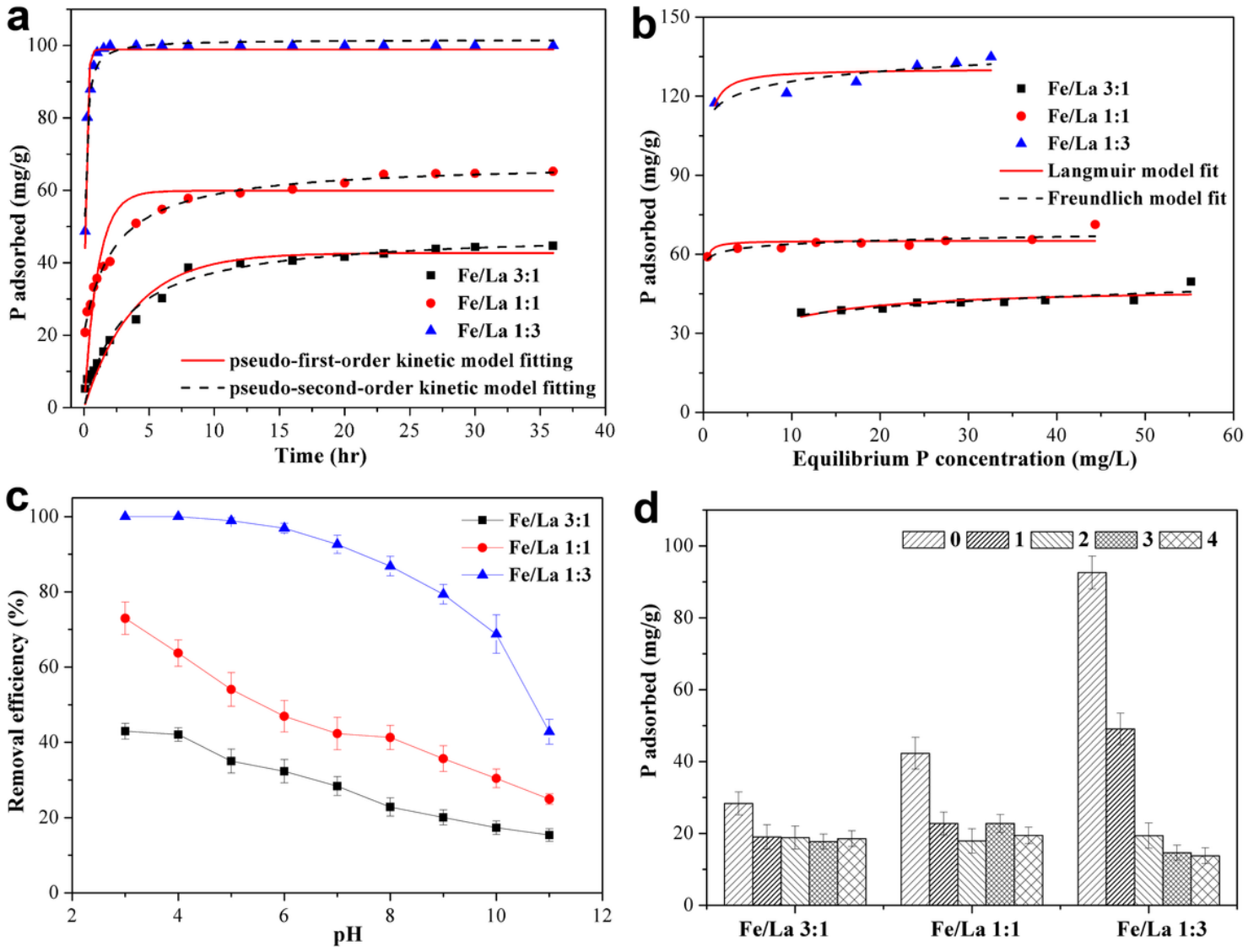

Figure 4

Phosphate adsorption performance of Fe-La binary (hydr)oxides. (a) Effect of contact time on phosphate removal at pH 4.0 and their kinetic fitting curves. (b) Adsorption isotherms of phosphate at pH 4.0 with an adsorbent dose of 0.5 g/L. (c) Effect of solution pH on phosphate removal. (d) Regeneration and reusability of Fe/La 3:1, Fe/La 1:1 and Fe/La 1:3 binary (hydr)oxides at pH 7.0 (the numbers of 0–4 represent the number of regeneration cycles). The initial phosphate concentration was 50.0 mg/L, and the adsorbent dose was 0.5 g/L.

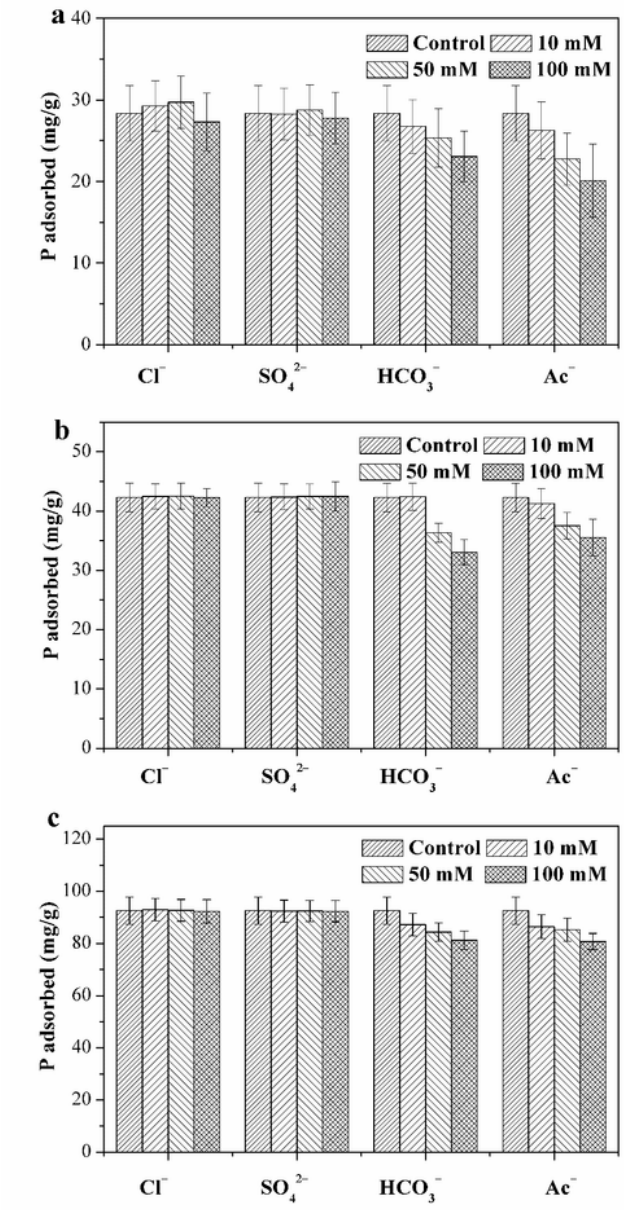

Figure 5

Effects of co-existing anions on the phosphate adsorption capacity of Fe/La 3:1 (a), Fe/La 1:1 (b) and Fe/La 1:3 (c) binary (hydr)oxides. The initial phosphate concentration was 50.0 mg/L, the solution pH was 7.0, and the adsorbent dose was 0.5 g/L.

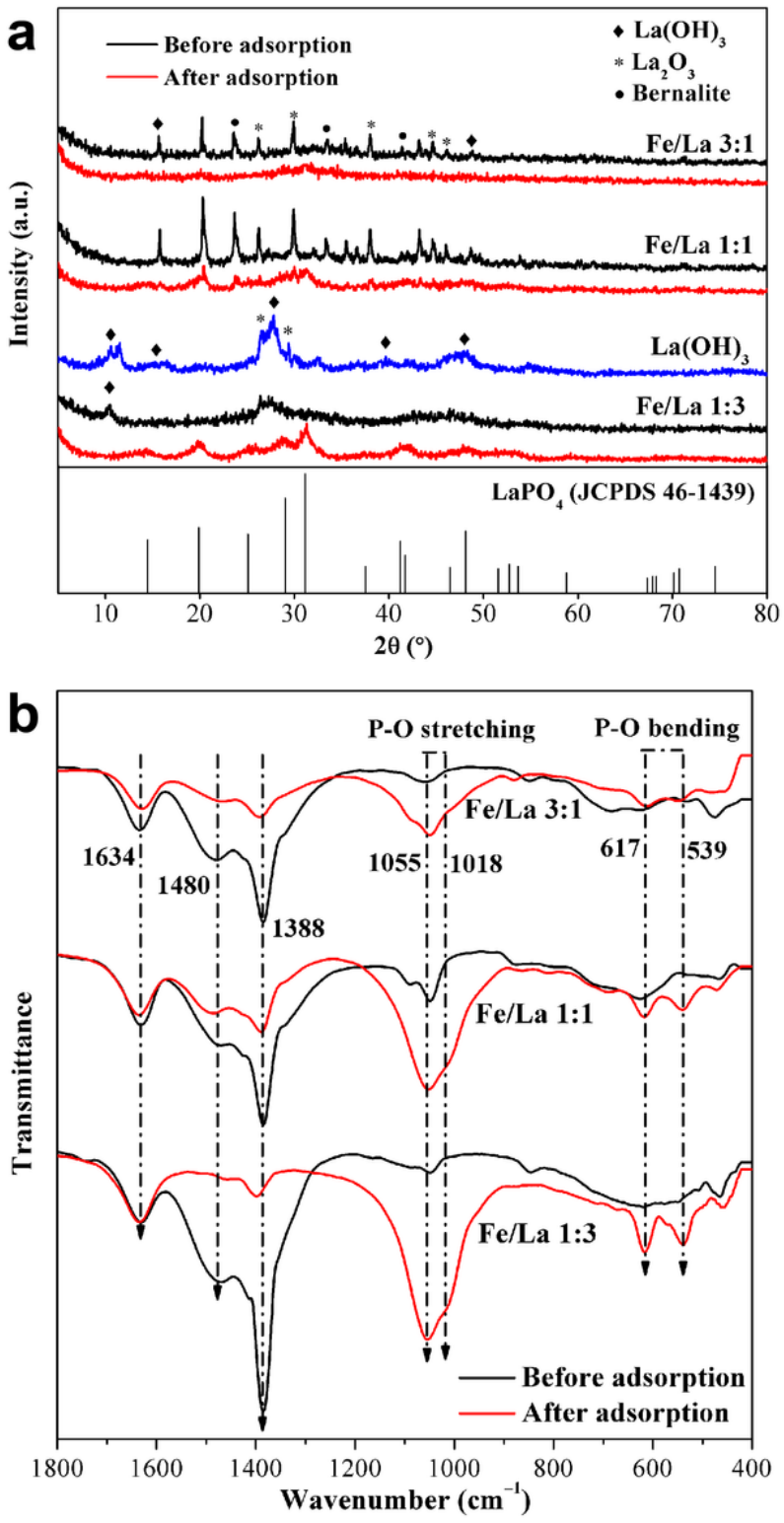

Figure 6

p-XRD patterns (a) and magnified FTIR spectra (b) of Fe/La 3:1, Fe/La 1:1 and Fe/La 1:3 binary (hydr)oxides before and after phosphate adsorption. The p-XRD pattern of the synthesized lanthanum hydroxide is also presented for comparison.

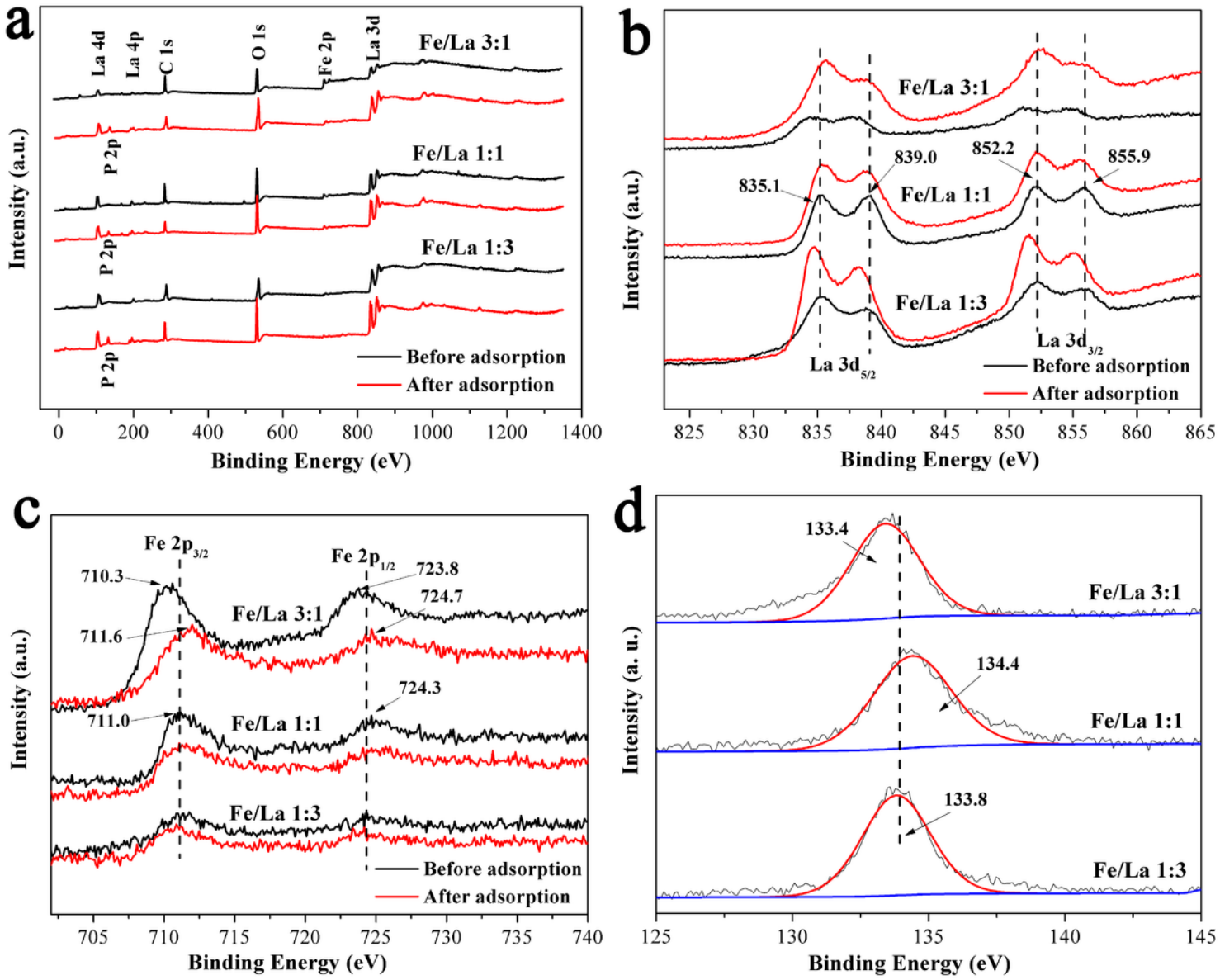

Figure 7

Survey (a), La 3d (b) and Fe 2p (c) XPS spectra of Fe/La 3:1, Fe/La 1:1 and Fe/La 1:3 binary (hydr)oxides before and after phosphate adsorption. P 2p (d) XPS spectra after phosphate adsorption.

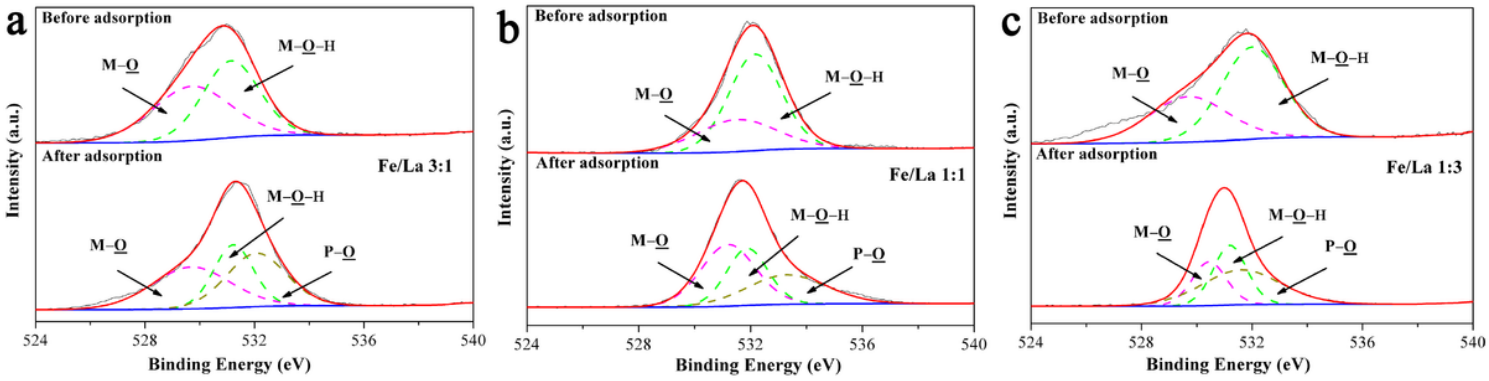

Figure 8

O 1s XPS spectra of Fe/La 3:1 (a), Fe/La 1:1 (b) and Fe/La 1:3 (c) binary (hydr)oxides before and after phosphate adsorption.

Supplementary Files

This is a list of supplementary files associated with this preprint. Click to download.

- AppendixA.docx